Available online at www.sciencedirect.com
SCIENCE DIRECT®
Journal of Solid State Chemistry 177 (2004) 293–298
JOURNAL OF SOLID STATE CHEMISTRY
http://elsevier.com/locate/jssc

# Structure and electrical resistivity of $CeNiSb_3$

Robin T. Macaluso,[a] Daniel M. Wells,[b] Richard E. Sykora,[b] Thomas E. Albrecht-Schmitt,[b] Arthur Mar,[c] S. Nakatsuji,[d] H. Lee,[d] Z. Fisk,[d] and Julia Y. Chan[a,*]

[a] *Department of Chemistry, Louisiana State University, 232 Choppin Hall, Baton Rouge, LA 70803, USA*
[b] *Department of Chemistry, Auburn University, Auburn, AL 36849, USA*
[c] *Department of Chemistry, University of Alberta, Edmonton, Alberta, Canada T6G 2G2*
[d] *National High Magnetic Field Laboratory, Florida State University, Tallahassee, FL 32306, USA*

Received 7 May 2003; received in revised form 12 August 2003; accepted 19 August 2003

**Abstract**

The ternary antimonide $CeNiSb_3$ has been prepared from an Sb flux or from reaction of Ce, NiSb, and Sb above 1123 K. It crystallizes in the orthorhombic space group *Pbcm* with $Z=12$ and lattice parameters $a=12.6340(7)$ Å, $b=6.2037(3)$ Å, and $c=18.3698(9)$ Å at 193 K. Its structure consists of buckled square nets of Sb atoms and layers of highly distorted edge- and face-sharing $NiSb_6$ octahedra. Located between the $^2_\infty[Sb]$ and $^2_\infty[NiSb_2]$ layers are the Ce atoms, in monocapped square antiprismatic coordination. There is an extensive network of Sb–Sb bonding with distances varying between 3.0 and 3.4 Å. The structure is related to that of $RECrSb_3$ but with a different stacking of the metal-centered octahedra. Resistivity measurements reveal a shallow minimum near 25 K that is suggestive of Kondo lattice behavior, followed by a sharp decrease below 6 K.


*Keywords:* Cerium; Nickel; Antimonide; Crystal structure; Resistivity

## 1. Introduction

Rare-earth antimonides, particularly multinary phases containing transition metals, have elicited intense interest because of their important physical properties and unusual bonding. Colossal magnetoresistance has been identified in $Eu_{14}MnSb_{11}$ [1,2], and relatively simple binary antimonides, such as $CeSb_2$ and $LaSb_2$, have remarkably complex and highly anisotropic magnetic and magnetoresistance properties [3]. Pronounced *f–p* and *f–d* hybridization is believed to mediate magnetic exchange mechanisms in phases such as $UMSb_2$ ($M$ = Fe, Co, Ni, Cu, Ru, Pd, Ag, Au) [4] and CeNiSb [5]. Itinerant electron ferromagnetism has been found in $LaCrSb_3$ and related phases [6].

An emerging feature in the structural chemistry of antimonides is the role of Sb–Sb bonds of variable strength in the formation of diverse anionic substructures such as discrete pairs (e.g., in $Yb_5In_2Sb_6$) [7], one-dimensional chains and ribbons (e.g., in $La_{13}Ga_8Sb_{21}$ and $Pr_{12}Ga_4Sb_{23}$) [8,9], and most pertinent to the present work, square nets (e.g., in $LaSn_{0.7}Sb_2$) [10]. These square nets appear frequently not only in antimonides, but also in other heavier pnictides, chalcogenides, and tetrelides. Application of the Zintl concept and other theoretical considerations suggest that a stable electron count for such square nets is six electrons per atom [11]. However, a $^2_\infty[Sb]^{1-}$ net is prone to distortion, and the resulting changes in the electronic structure affect the electrical and magnetic properties.

Herein we report the synthesis, structure, and electrical resistivity of $CeNiSb_3$. Its structure is related to that of $REVSb_3$ and $RECrSb_3$ [12,13] but with more varied Sb–Sb bonding interactions.

## 2. Experimental

### 2.1. Synthesis

$CeNiSb_3$ can be synthesized by two methods, both of which are discussed. The single crystal used for X-ray

*Corresponding author. Fax: +1-225-578-3458.
*E-mail address:* jchan@lsu.edu (J.Y. Chan).

0022-4596/$ - see front matter © 2003 Elsevier Inc. All rights reserved.
doi:10.1016/j.jssc.2003.08.020

diffraction experiments was isolated from the reaction of Ce (99.9%, Alfa-Aesar), NiSb (99.5%, Alfa-Aesar), and Sb (99.5%, Alfa-Aesar) which were loaded in a fused-silica tube in a molar ratio of 1:2:5. The tube was sealed under vacuum and heated at 1123 K for 7 days followed by annealing at 873 K for 5 days. The tube was then cooled at $0.5\,K\,min^{-1}$ to room temperature. The product consisted of excess Sb, black needles of $NiSb_2$, and black tablets of $CeNiSb_3$. Crystals of $CeNiSb_3$ up to 1 mm in length and uncontaminated with $NiSb_2$ could be isolated from the reaction of Ce, NiSb, and Sb in a 1:1:2 ratio under the same heating conditions but with the cooling rate reduced to $0.25\,K\,min^{-1}$.

Large, high-quality single crystals of $CeNiSb_3$ were also synthesized by a flux growth method. Ce ingot (99.95%, Ames Laboratory), Ni (99.995%, Alfa-Aesar), and Sb (99.9999%, Alfa-Aesar) were placed in an alumina crucible in a 1:2:20 ratio. The crucible and its contents were sealed in an evacuated fused-silica tube. The entire reaction vessel was heated to 1373 K where the temperature was maintained for 2 h and then cooled to 943 K at $5\,K\,h^{-1}$, at which point excess Sb flux was separated by centrifugation. Plate-like crystals with dimensions up to $2\times2\times1\,mm^3$ were mechanically separated from the alumina crucible for analysis. The crystals are stable in air and do not degrade noticeably.

Semi-quantitative SEM/EDX analysis was performed on crystals of $CeNiSb_3$ with use of a JEOL 840/Link Isis instrument. Ce, Ni, and Sb percentages were calibrated against standards and a Ce:Ni:Sb ratio of 1:1:3 was found.

### 2.2. Single crystal X-ray diffraction

A tabular crystal of $CeNiSb_3$ with dimensions of $0.112\times0.020\times0.048$ mm and faces indexed as {100}, {010}, and {001} was mounted on a glass fiber with epoxy and aligned on a Bruker SMART APEX CCD X-ray diffractometer. Data were collected at 193 K with use of graphite monochromated Mo$K\alpha$ radiation from a sealed tube equipped with a monocapillary collimator. SMART was used for preliminary determination of the cell constants and data collection control. Intensities were collected by a combination of three sets of exposures (frames). Each set had a different $\phi$ angle for the crystal and each exposure covered a range of 0.3° in $\omega$. A total of 1800 frames were collected with an exposure time per frame of 30 s.

Data were processed with the Bruker SAINT (v. 6.02) software package using a narrow-frame integration algorithm. A face-indexed analytical absorption correction was initially applied using XPREP [14]. Individual shells of unmerged data were corrected analytically and exported in the same format. These files were subsequently treated with a semi-empirical absorption correction by SADABS [15]. The program suite SHELXTL (v. 6.12) was used for space group determination (XPREP), direct methods structure solution (XS), and least-squares refinement (XL) [14]. The final refinements included anisotropic displacement parameters for all atoms and a secondary extinction parameter. Crystallographic details are listed in Table 1. Atomic positions and displacement parameters are listed in Table 2, and interatomic distances are listed in Table 3. Further details of the crystal structure investigation may be obtained from Fachinformationszentrum Karlsruhe, D-76344 Eggenstein-Leopoldshafen, Germany (Fax: (+49)7247-808-666; e-mail: crysdata@fiz-karlsruhe.de) on quoting the depository number CSD-39122.

### 2.3. Electrical resistivity

The electrical resistivity of a single crystal of $CeNiSb_3$ along the crystallographic $b$-axis was measured by standard four-probe ac methods between 300 and 0.6 K using a Quantum Design PPMS instrument. Measurement on another crystal of similar dimensions confirmed that the results were reproducible.

Table 1
Crystallographic data for $CeNiSb_3$

| | |
|---|---|
| Formula | $CeNiSb_3$ |
| Formula mass (amu) | 564.08 |
| Space group | *Pbcm* (No. 57) |
| $a$ (Å) | 12.6340(7) |
| $b$ (Å) | 6.2037(3) |
| $c$ (Å) | 18.3698(9) |
| $V$ (Å$^3$) | 1439.78(13) |
| $Z$ | 12 |
| $T$ (K) | 193 |
| $\rho_{calcd}$ (g cm$^{-3}$) | 7.807 |
| Crystal dimensions (mm) | $0.112\times0.048\times0.020$ |
| Radiation | Graphite monochromated Mo$K\alpha$, $\lambda = 0.71073$ Å |
| $\mu$(Mo$K\alpha$) (cm$^{-1}$) | 296.1 |
| Transmission factors | 0.0362–0.5562 |
| $2\theta$ limits | $3.22° \leqslant 2\theta(\text{Mo}K\alpha) \leqslant 56.54°$ |
| Data collected | $-16 \leqslant h \leqslant 16$, $-8 \leqslant k \leqslant 8$, $-24 \leqslant l \leqslant 24$ |
| No. of data collected | 13873 |
| No. of unique data, including $F_o^2 < 0$ | 1845 ($R_{int}$ = 0.0364) |
| No. of unique data, with $F_o^2 > 2\sigma(F_o^2)$ | 1730 |
| No. of variables | 75 |
| $R(F)$ for $F_o^2 > 2\sigma(F_o^2)$[a] | 0.0188 |
| $R_w(F_o^2)$[b] | 0.0433 |
| Goodness of fit | 1.111 |
| $(\Delta\rho)_{max}$, $(\Delta\rho)_{min}$ ($e$ Å$^{-3}$) | 1.109, −1.123 |

[a] $R(F) = \sum ||F_o| - |F_c|| / \sum |F_o|$ .

[b] $R_w(F_o^2) = [\sum[w(F_o^2 - F_c^2)^2] / \sum wF_o^4]^{1/2}$; $w^{-1} = [\sigma^2(F_o^2) + (0.0163p)^2 + 4.4358p]$, where $p = [\max(F_o^2, 0) + 2F_c^2]/3$.

Table 2
Atomic coordinates and equivalent isotropic displacement parameters for $CeNiSb_3$

| Atom | Wyckoff position | $x$ | $y$ | $z$ | $U_{eq}$ (Å$^2$)[a] |
|---|---|---|---|---|---|
| Ce1 | 4*d* | 0.30554(3) | –0.05700(6) | 1/4 | 0.00707(9) |
| Ce2 | 8*e* | 0.29911(2) | 0.47384(4) | 0.416578(13) | 0.00707(7) |
| Ni1 | 4*c* | –0.10166(7) | 1/4 | 1/2 | 0.00789(17) |
| Ni2 | 8*e* | –0.09777(5) | 0.67164(10) | 0.17593(3) | 0.00961(13) |
| Sb1 | 8*e* | 0.49648(2) | 0.20701(5) | 0.334051(16) | 0.00807(8) |
| Sb2 | 4*d* | 0.21934(3) | 0.44721(7) | 1/4 | 0.00790(10) |
| Sb3 | 4*c* | 0.50405(3) | 1/4 | 1/2 | 0.00826(10) |
| Sb4 | 8*e* | 0.22356(3) | 0.52537(5) | 0.584227(16) | 0.00759(8) |
| Sb5 | 8*e* | –0.02613(3) | 0.54305(5) | 0.586595(16) | 0.00785(8) |
| Sb6 | 4*d* | 0.05847(3) | 0.81154(7) | 1/4 | 0.00776(10) |

[a] $U_{eq}$ is defined as one-third of the trace of the orthogonalized $U_{ij}$ tensor.

Table 3
Selected interatomic distances (Å) in $CeNiSb_3$

| | | | |
|---|---|---|---|
| Ce1–Sb4 ( × 2) | 3.2225(3) | Ni2–Sb6 | 2.5498(7) |
| Ce1–Sb6 | 3.2262(6) | Ni2–Sb5 | 2.5778(7) |
| Ce1–Sb1 ( × 2) | 3.2838(5) | Ni2–Sb4 | 2.6186(7) |
| Ce1–Sb1 ( × 2) | 3.2994(4) | Ni2–Sb5 | 2.6301(7) |
| Ce1–Sb2 | 3.2629(6) | Ni2–Sb6 | 2.6624(7) |
| Ce1–Sb2 | 3.3112(6) | Ni2–Sb2 | 2.6708(7) |
| Ce1–Ni2 ( × 2) | 3.2793(7) | Ni2–Ni2 | 2.7214(12) |
| Ce2–Sb2 | 3.2260(3) | Sb1–Sb3 | 3.0616(3) |
| Ce2–Sb4 | 3.2400(4) | Sb1–Sb1 | 3.0880(6) |
| Ce2–Sb4 | 3.2408(4) | Sb1–Sb1 ( × 2) | 3.1031(2) |
| Ce2–Sb4 | 3.2501(4) | Sb2–Sb6 | 3.0395(6) |
| Ce2–Sb3 | 3.3137(4) | Sb3–Sb1 ( × 2) | 3.0616(3) |
| Ce2–Sb1 | 3.3256(4) | Sb3–Sb3 ( × 2) | 3.1035(2) |
| Ce2–Sb1 | 3.3550(4) | Sb4–Sb5 | 3.1568(5) |
| Ce2–Sb3 | 3.3864(4) | Sb5–Sb4 | 3.1568(5) |
| Ce2–Sb5 | 3.4509(4) | Sb5–Sb5 ( × 2) | 3.1714(2) |
| Ce2–Ni1 | 3.3921(7) | Sb5–Sb5 | 3.2929(6) |
| Ni1–Sb4 ( × 2) | 2.5899(6) | Sb5–Sb6 | 3.3116(4) |
| Ni1–Sb5 ( × 2) | 2.5973(4) | Sb6–Sb2 | 3.0395(6) |
| Ni1–Sb5 ( × 2) | 2.6049(6) | Sb6–Sb5 ( × 2) | 3.3116(4) |
| | | Sb6–Sb6 ( × 2) | 3.4358(6) |

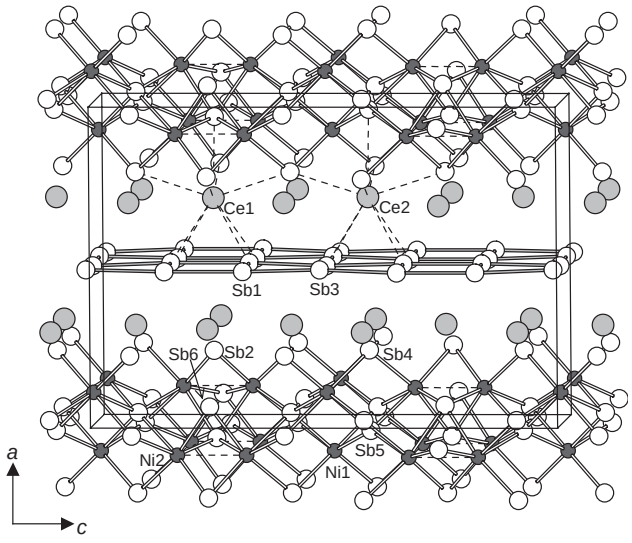


Fig. 1. View down the *b*-axis of $CeNiSb_3$ with the unit cell outlined. The large shaded circles are Ce atoms, the small solid circles are Ni atoms, and the medium open circles are Sb atoms. The coordination around the two crystallographically inequivalent Ce atoms is shown by dashed lines. The short 2.7214(12) Å distances between pairs of Ni2 atoms across the shared face of octahedra are indicated by horizontal dashed lines.

## 3. Results and discussion

### 3.1. Structure

$CeNiSb_3$ crystallizes in a new structure type. As shown in Fig. 1, the structure can be viewed as being built up by inserting Ce atoms between a layer of condensed Ni-centered octahedra, $^2_\infty[NiSb_2]$, and a buckled, nearly square net, $^2_\infty[Sb]$. There are also additional Sb–Sb interactions within the $^2_\infty[NiSb_2]$ layer.

Each of the two crystallographically inequivalent Ce atoms is nine-coordinate and adopts a monocapped square antiprismatic geometry, in which four Sb atoms in the $^2_\infty[Sb]$ net form a square base, four Sb atoms in the $^2_\infty[NiSb_2]$ layer form a larger square twisted 45° relative to the first, and one Sb atom caps this larger square (Fig. 1). The Ce atoms are located above and below the $^2_\infty[Sb]$ square net in a "checkerboard" pattern. The Ce1–Sb distances of 3.2225(3)–3.3112(6) Å and the Ce2–Sb distances of 3.2260(3)–3.4509(4) Å are comparable to those in $CeCrSb_3$ (3.259(1)–3.334(1) Å) where the Ce atoms have a similar coordination geometry [12].

The $^2_\infty[NiSb_2]$ layer contains two kinds of Ni-centered octahedra, $Ni1(Sb4)_{2/2}(Sb5)_{4/4}$ and $Ni2(Sb2)_{1/2}(Sb4)_{1/2}(Sb5)_{2/4}(Sb6)_{2/4}$, that share edges in the *b*-direction and both edges and faces in the *c*-direction. The Ni1–Sb distances of 2.5899(6)–2.6049(6) Å and the Ni2–Sb distances of 2.5498(7)–2.6708(7) Å are similar to the average Ni–Sb distance of 2.608 Å in NiSb (NiAs-type) where octahedrally coordinated Ni is also found [16,17]. These octahedra are highly distorted, with Sb–Ni–Sb angles as acute as 136.89(4)° and 146.72(3)° subtending *trans* Sb atoms about the Ni1 and Ni2 atoms, respectively. Associated with this distortion is the occurrence of a short Ni2–Ni2 distance of 2.7214(12) Å

within a pair of face-sharing octahedra (dashed horizontal lines in Fig. 1).

The $^2_\infty$[Sb] net is formed by four-bonded Sb1 and Sb3 atoms (Fig. 2a). Whereas the Sb atoms are spaced regularly along the *b*-direction (Sb1–Sb1, 3.1031(2) Å; Sb3–Sb3, 3.1035(2) Å), there are small distortions along the *c*-direction (Sb1–Sb3, 3.0616(3) Å; Sb1–Sb1, 3.0880(6) Å). There is a slight buckling of the $^2_\infty$[Sb] net so that the Sb1 and Sb3 atoms are displaced above or below the mean plane by ~0.05 Å. The net is not strictly square, with Sb–Sb–Sb angles ranging from 84.95(1)° to 94.94(1)°.

Extensive Sb–Sb interactions also pervade the $^2_\infty$[$NiSb_2$] layer, with distances ranging from 3.0395(6) to 3.4358(6) Å (Fig. 2b). This Sb substructure can be roughly described as a three-layer stacking of $4^4$ nets. The two peripheral nets (made up of Sb2 and Sb4 atoms) are half as dense as and rotated by 45° to the intervening net made up of Sb5 and Sb6 atoms. If an arbitrary cutoff of 3.2 Å is used, Sb2–Sb6 pairs (3.0395(6) Å) and one-dimensional bands of Sb4 and Sb5 atoms (Sb4–Sb5, 3.1568(5) Å; Sb5–Sb5, 3.1714(2) Å) become evident.

### 3.2. Structural relationships

In previously known Ce–Ni–Sb phases, the Ni atoms are in trigonal planar (CN3 in CeNiSb (ZrBeSi-type)), tetrahedral (CN4 in $CeNiSb_2$ ($ZrCuSi_2$-type) and $CeNi_{2-x}Sb_2$ ($CaBe_2Ge_2$-type)), or square pyramidal (CN5 in $CeNi_{2-x}Sb_2$ ($CaBe_2Ge_2$-type)) coordination [18–20]. In contrast, the Ni atoms are in octahedral coordination (CN6) in $CeNiSb_3$. The structures of $CeNiSb_3$ and $CeNiSb_2$ are related in that the layers of Ni-centered octahedra $^2_\infty$[$NiSb_2$] in $CeNiSb_3$ are replaced by layers of Ni-centered tetrahedra $^2_\infty$[NiSb] in $CeNiSb_2$ [19], with the $^2_\infty$[Sb] net and the arrangement of Ce atoms remaining intact. A closer relationship is found with the ternary rare-earth antimonides *RE*$VSb_3$ and *RE*$CrSb_3$ (for concreteness, $CeCrSb_3$ is shown in Fig. 3a) [6,12,13]. In $CeCrSb_3$, chains of face-sharing metal-centered octahedra extend along the *c*-direction; these chains are connected by edge-sharing in the *b*-direction to form a $^2_\infty$[$CrSb_2$] layer parallel to the *bc*-plane (Fig. 3a). In $CeNiSb_3$, every third metal-centered octahedron in the chains extending along the *c*-direction is connected by edge-sharing instead of

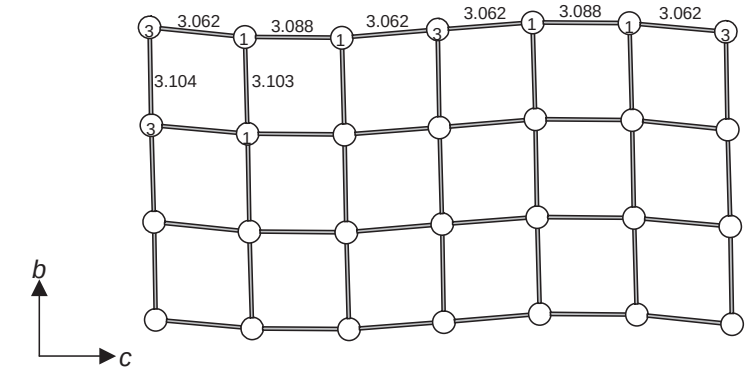


(a)

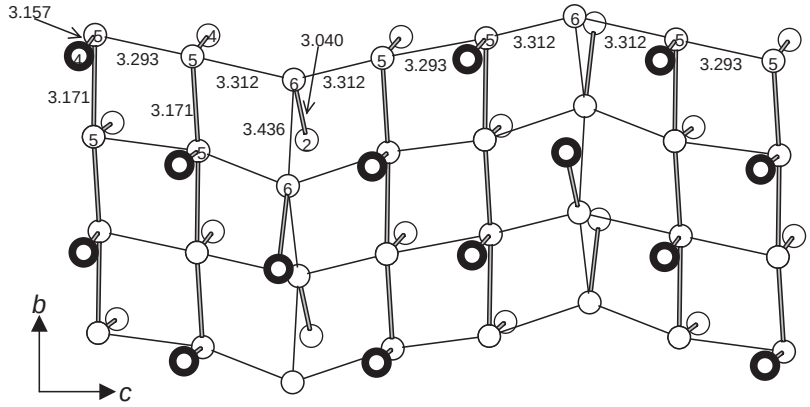


(b)

Fig. 2. Sb–Sb interactions within (a) the $^2_\infty$[Sb] square net and (b) the $^2_\infty$[$NiSb_2$] layer (with Ni atoms omitted), both extending infinitely parallel to the *bc*-plane. Distances are in Å and have standard uncertainties less than 0.001 Å. In (b), atoms with thicker rims are closer to the viewer.

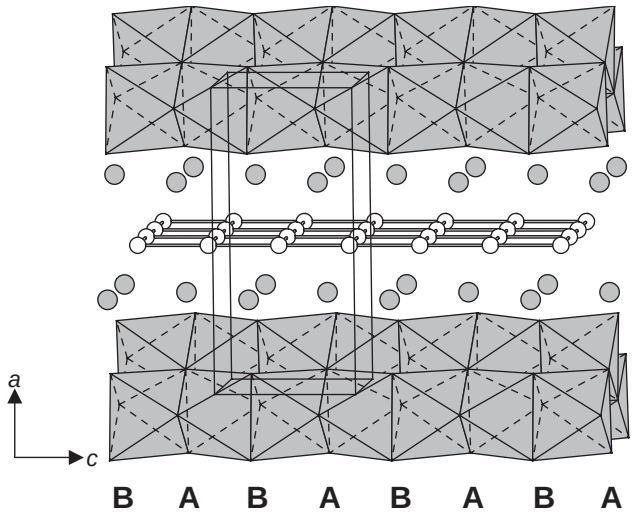


(a) $CeCrSb_3$

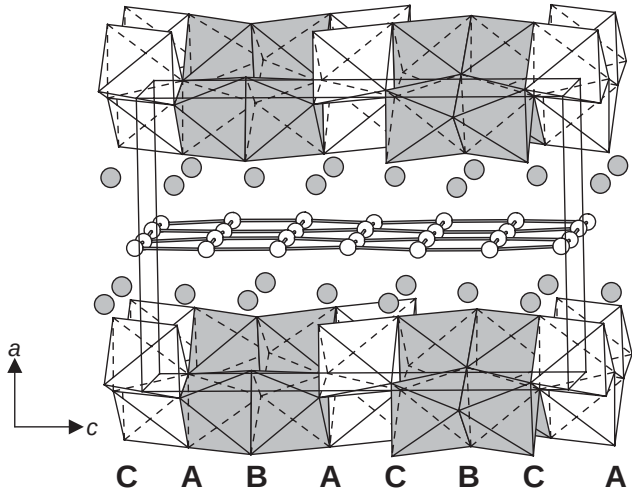


(b) $CeNiSb_3$

Fig. 3. Comparison of the structures of (a) $CeCrSb_3$ and (b) $CeNiSb_3$, both in space group *Pbcm*. The structures differ in the stacking sequence of metal-centered octahedra along the *c*-direction. Face-sharing octahedra are shaded.

face-sharing (Fig. 3b). The stacking sequence of the Sb atoms along the *c*-direction is AB in $CeCrSb_3$ and ABACBC in $CeNiSb_3$, or in Jagodzinski notation, *h* and *hcc*, respectively. $CeNiSb_3$ crystallizes in the same space group (*Pbcm*) as $CeCrSb_3$, but its *c* parameter is tripled, reflecting the more complicated stacking sequence.

### 3.3. Bonding

Interpretation of the bonding in $CeNiSb_3$ is complicated by the possibility of mixed $+3/+4$ valency on the Ce atoms, by the pairing of Ni atoms across the shared face of the octahedra, and by the rich variety of Sb–Sb interactions within the Sb substructure. The similarity of Ce–Sb distances in $CeNiSb_3$ to those in $CeCrSb_3$ argues for $Ce^{3+}$, and it is reasonable to assume that the Ce atoms participate, to a first approximation, in ionic interactions with the other atoms in the structure. The Ni2–Ni2 distance of 2.7214(12) Å is slightly longer than the analogous distance of ~2.560 Å found in NiSb [16,17], where metal–metal bonding has long been known to be important in stabilizing its structure [21]. Magnetic measurements might also clarify the oxidation state of the Ni atoms, but the assumption of localized moments is highly suspect given the observation of itinerant electron ferromagnetism in the related series of compounds *RE*$CrSb_3$ [6]. In the absence of additional experimental data, the Sb substructure can be analyzed as a starting point.

The Sb–Sb distances in $CeNiSb_3$ (3.0395(6)–3.4358(6) Å) are longer than the intralayer distance (2.908 Å) and comparable to the interlayer distance (3.355 Å) found in elemental Sb [22]. The four-bonded Sb atoms within the $^2_\infty$[Sb] square net can be assigned oxidation numbers of –1, if the Sb–Sb interactions are considered to be one-electron bonds and two lone pairs are localized on each atom so that an octet is attained. For the Sb atoms within the $^2_\infty$[$NiSb_2$] layer, however, the assumption of integral oxidation numbers breaks down. An elegant way, proposed by Jeitschko et al., to enumerate electrons within such complex Sb substructures is to apply a bond valence calculation to derive formal charges on these Sb atoms [23]. When bond orders are calculated from the equation $v_{ij} = \exp[(2.80-d_{ij})/0.37]$ (where $d_{ij}$ is in Å), the formal charges of the Sb atoms in $CeNiSb_3$ are found to be $-1.2$ on Sb1, $-2.5$ on Sb2, $-1.1$ on Sb3, $-2.6$ on Sb4, $-1.4$ on Sb5, and $-1.6$ on Sb6. The charges on Sb1 and Sb3 are consistent with those in the simple model of one-electron bonds in a $^2_\infty$[Sb] square net (Fig. 2a). The one-bonded Sb2 and Sb4 atoms (Fig. 2b) carry the most negative charges, whereas the Sb5 and Sb6 atoms have intermediate charges between these extremes. If these formal charges are rounded off to the nearest half-integer and when the multiplicity of atomic sites is taken into account, the total negative charge of approximately $-60$ on the Sb atoms within a unit cell can be compensated by assuming $+3$ charges on the Ce atoms and $+2$ charges on the Ni atoms: $(Ce^{3+})_{12}(Ni^{2+})_{12}(Sb_{36})^{60-}$ or $Ce^{3+}Ni^{2+}(Sb_3)^{5-}$. It is important to appreciate that the true charges are not likely to be as extreme as implied by these formulations. The caveat about the dangers of assuming a localized electron model has already been mentioned, and significant covalent character is expected in the Ni–Sb and perhaps even the Ce–Sb bonds. It would be interesting to perform a band structure calculation to understand the bonding in more detail.

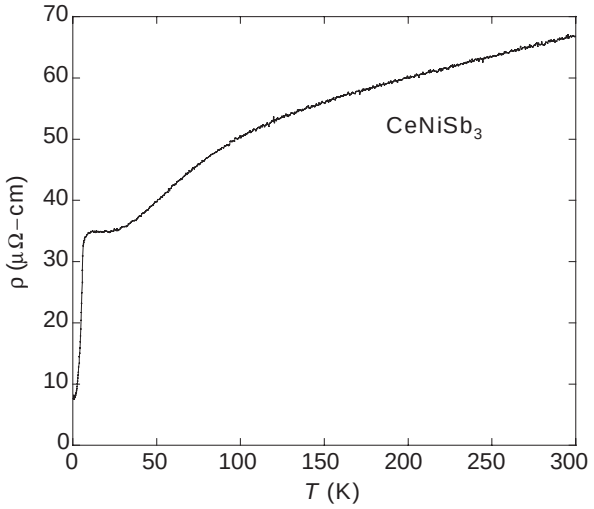


Fig. 4. Electrical resistivity of $CeNiSb_3$ between 0.6 and 300 K along the *b*-axis.

### 3.4. Electrical resistivity

Fig. 4 shows the temperature dependence of the electrical resistivity of a single crystal of $CeNiSb_3$ along the *b*-axis. Metallic behavior is observed with a prominent curvature in the plot, which exhibits a minimum near 25 K, followed by a steep decrease at 6 K. This behavior is typical of magnetically ordered Kondo lattices with a localized *f* moment weakly coupled to the conduction bands. The resistivity plot bears a striking resemblance to that of $CeSn_{0.7}Sb_2$, a ferromagnetic layered antimonide with a similar arrangement of Ce atoms and Ce–Ce distances as in $CeNiSb_3$. It is likely that the transitions in the resistivity curve can be attributed to the Ce moments. Further experiments to measure the magnetic and transport properties would be helpful in clarifying the electronic structure of $CeNiSb_3$.

## Acknowledgments

T.A.-S. acknowledges the U.S. Department of Energy through Grant DE-FG02-02ER45963 for support of this work. Z.F. acknowledges NSF DMR-9971348, and J.Y.C. acknowledges Petroleum Research Fund and National Science Foundation CAREER DMR#0237664.

## References

[1] S.M. Kauzlarich, Chemistry, Structure and Bonding of Zintl Phases and Ions, VCH Publishers, New York, 1996.
[2] J.Y. Chan, S.M. Kauzlarich, P. Klavins, R.N. Shelton, D.J. Webb, Chem. Mater. 9 (1997) 3132.
[3] S.L. Bud'ko, P.C. Canfield, C.H. Mielke, A.H. Lacerda, Phys. Rev. B 57 (1998) 13624.
[4] D. Kaczorowski, R. Kruk, J.P. Sanchez, B. Malaman, F. Wastin, Phys. Rev. B 58 (1998) 9227.
[5] I. Karla, J. Pierre, R.V. Skolozdra, J. Alloys Compd. 265 (1998) 42.
[6] N.P. Raju, J.E. Greedan, M.J. Ferguson, A. Mar, Chem. Mater. 10 (1998) 3630.
[7] S.-J. Kim, J.R. Ireland, C.R. Kannewurf, M.G. Kanatzidis, J. Solid State Chem. 155 (2000) 55.
[8] A.M. Mills, L. Deakin, A. Mar, Chem. Mater. 13 (2001) 1778.
[9] A.M. Mills, R. Lam, M.J. Ferguson, L. Deakin, A. Mar, Coord. Chem. Rev. 233–234 (2002) 207.
[10] L. Deakin, M.J. Ferguson, M.J. Sprague, A. Mar, R.D. Sharma, C.H.W. Jones, J. Solid State Chem. 164 (2002) 292.
[11] G.A. Papoian, R. Hoffmann, Angew. Chem. Int. Ed. 39 (2000) 2408.
[12] M. Brylak, W. Jeitschko, Z. Naturforsch. B: Chem. Sci. 50 (1995) 899.
[13] M.J. Ferguson, R.W. Hushagen, A. Mar, J. Alloys Compd. 249 (1997) 191.
[14] G.M. Sheldrick, SHELXTL PC, Version 6.12, An Integrated System for Solving, Refining, and Displaying Crystal Structures from Diffraction Data, Siemens Analytical X-ray Instruments, Inc., Madison, WI, 2001.
[15] R.H. Blessing, SADABS, Program for absorption correction using SMART CCD based on the method of Blessing, 1995.
[16] N. Alsen, Geol. Foren. Stock. Forh. 47 (1925) 19.
[17] T. Chen, J.J.C. Mikkelsen, G.B. Charlan, J. Cryst. Growth 43 (1978) 5.
[18] V.K. Pecharskii, Yu.V. Pankevich, O.I. Bodak, Kristallografiya 28 (1983) 173.
[19] Yu.V. Pankevich, V.K. Pecharskii, O.I. Bodak, Izv. Akad. Nauk SSSR Metally (1983) 227.
[20] W.K. Hofmann, W. Jeitschko, J. Less-Common Metals 138 (1988) 313.
[21] W. Tremel, R. Hoffmann, J. Silvestre, J. Am. Chem. Soc. 108 (1996) 5174.
[22] J. Donohue, The Structures of the Elements, Wiley, New York, 1974.
[23] W. Jeitschko, R.O. Altmeyer, M. Schelk, U.C. Rodewald, Z. Anorg. Allg. Chem. 627 (2001) 1932.